
Article:
Bailey, D.J. orcid.org/0000-0002-0313-8748, Gardner, L.J. orcid.org/0000-0003-3126-2583, Harrison, M.T. et al. (2 more authors) (2022) Development of monazite glass-ceramic wasteforms for the immobilisation of pyroprocessing wastes. MRS Advances, 7 (5-6). pp. 81-85.

https://doi.org/10.1557/s43580-022-00230-5

MRS Advances (2022) 7:81–85
https://doi.org/10.1557/s43580-022-00230-5

ORIGINAL PAPER

Development of monazite glass-ceramic wasteforms for the immobilisation of pyroprocessing wastes

D. J. Bailey[1] · L. J. Gardner[1] · M. T. Harrison[2] · D. McKendrick[2] · N. C. Hyatt[1]

Received: 30 November 2021 / Accepted: 2 February 2022 / Published online: 9 March 2022

Abstract

Pyrochemical reprocessing is a potential route for the reprocessing of fuels from next-generation reactors. Lanthanide fission products may be separated from the reprocessing salt by a number of methods; however, salts may be entrained in the resultant product. This work demonstrates conceptual monazite glass-ceramic wasteforms based on the quarternary $(100-x)(10Na_2O–36Fe_2O_3–54P_2O_5)–xLa_2O_3$ ($x = 5, 10, 15$), with La_2O_3 as a surrogate for the lanthanide oxide waste stream. Samples were produced by the melting of La_2O_3 with a sodium-iron-phosphate glass frit and characterised by XRD and SEM–EDX. The monazite phase was successfully formed at all waste loadings with clear segregation of La to the crystalline phase; however, high La_2O_3 loading (>10 mol%) was found to destabilise the glass system resulting in gross crystallisation. These initial results indicate that monazite glass-ceramics are promising wasteforms for this waste stream.

Introduction

There is a resurgence of interest in the pyrochemical reprocessing (pyroprocessing) of spent nuclear fuels in the context of Generation IV reactor systems, which may not be compatible with aqueous reprocessing flowsheets. In this approach, the spent fuel is dissolved in a LiCl–KCl eutectic salt (LKE, $Li_{0.48}K_{0.52}Cl$), with electrochemical separation of uranium and plutonium from the fission products [1, 2]. The LKE salt is resistant to radiolysis and thus better suited to high burn up and short cooled nuclear fuels, compared to aqueous solvent extraction; additionally, co-extraction of uranium and plutonium offers enhanced proliferation resistance [1, 2]. Periodically, the LKE salt will require decontamination of fission products to maintain efficiency. One approach for removal of the lanthanide fission products is oxidative precipitation, to yield Ln_2O_3, LnOCl, or a mixture thereof, depending on the reaction conditions, which may be achieved by oxygen sparging of the LKE molten salt [3–5] according to the following reactions [6]:

$$2\,LnCl_3 + O_{2(g)} \rightarrow 2\,LnOCl + 2Cl_{2(g)}$$

$$4\,LnOCl + O_{2(g)} \rightarrow 2\,Ln_2O_3 + 2Cl_{2(g)}$$

$$2\,LnOCl + O_{2(g)} \rightarrow 2LnO_2 + Cl_{2(g)}$$

Assuming reaction completion to yield precipitated lanthanide oxides, the waste stream may be reasonably expected to carry entrained LKE salt and other potential fission products. Consequently, a glass-ceramic wasteform may be appropriate for this waste stream, with a monazite $LnPO_4$ phase to immobilise the lanthanide, with entrained fission products and LKE salt immobilised in the glass phase. Accordingly, our interest is focussed on the potential of iron phosphate glass–monazite ceramic systems for this application, given the expected chemical compatibility of the monazite and phosphate glass components. Indeed, Asuvathraman et al. reported a monazite glass composite wasteform for the immobilisation of fission product HLW arising from aqueous reprocessing of fast breeder reactor fuel [7–11]. A monazite $Ca_{0.8}Ce_{0.2}PO_4$ host phase was first synthesised by a sol gel route, with the equivalent of 20 wt% of HLW fission products and minor actinides targeted for substitution on the Ca/Ce site. The powder material was mixed with 20 wt% $40Fe_2O_3–60P_2O_5$, to form an apparently durable glass composite. This approach is of interest since it demonstrates the apparent flexibility of the monazite phase

✉ D. J. Bailey
d.j.bailey@sheffield.ac.uk

[1] Immobilisation Science Laboratory, University of Sheffield, Sheffield S1 3JD, UK

[2] National Nuclear Laboratory, Central Laboratory, Sellafield, Seascale CA20 1PG, Cumbria, UK

towards incorporation of fission product elements. However, it would be preferable to produce such a glass-ceramic wasteform in a single one-pot process.

The quaternary systems $(100 - x)(36Fe_2O_3–10B_2O_3–54P_2O_5)–xLn_2O_3$ were reported to afford iron phosphate glass–monazite ceramic materials, according to the systematic studies of Wang et al. [8–11]. The $(100 - x)(36Fe_2O_3–10B_2O_3–54P_2O_5)–xCeO_2$ system was reported to be fully amorphous up to 9 mol% CeO_2 incorporation, above which monazite $CePO_4$ was crystallised, and additionally $FePO_4$ above 18 mol% [8]. Wang et al. also studied the $(100 - x)(36Fe_2O_3–10B_2O_3–54P_2O_5)–xLn_2O_3$ system, with Ln = Nd and La, which is described by a similar phase diagram with a fully amorphous material produced up to 4 mol% Ln_2O_3 incorporation, above which monazite $LnPO_4$ was crystallised [9, 10]. Wang et al. further reported the application of this conceptual wasteform to the immobilisation of a simulant high level waste (HLW) produced in China, rich in actinides, transuranics and molybdenum [11]. The formulation design was $(100 - x)(36Fe_2O_3–10B_2O_3–54P_2O_5)–x$HLW; an amorphous product was obtained up to 5 mol% incorporation, above which monazite (Ce,Nd,La)PO_4 was crystallised. Incorporation of CeO_2 and Ln_2O_3 in the quaternary systems did not markedly affect the glass dissolution rate relative to the base glass, which was of the order of 10^{-2} g m^{-2} day^{-1} as measured by total weight loss of monoliths in a batch dissolution experiment at 90 °C in deionised water. However, incorporation of the HLW simulant reduced the dissolution rate to the order of 10^{-3}–10^{-4} g m^{-2} day^{-1}, likely due to the formation of hydration-resistant Zr-O-P bonds.

Deng et al. investigated the $(100 - x)(40Fe_2O_3–60P_2O_5)–xCeO_2$ system and established the crystallisation of monazite $CePO_4$ above 4 mol% CeO_2 incorporation [12]. In comparison with the data of Wang et al., this demonstrates that the addition of B_2O_3 to the $40Fe_2O_3–60P_2O_5$ base glass increases the solubility of CeO_2. Deng et al. reported very low dissolution rates of ~ 10^{-5} g m^{-2} day^{-1} for such iron phosphate glass–monazite ceramics in PCT experiments with deionised water at 90 °C, based on chemical analysis of solutions.

As noted above, precipitation of lanthanide oxide fission products by oxygen sparging of LKE in salt clean-up from pyroprocessing may be reasonably expected to carry entrained LKE salt and other fission products into the wasteform process. We have previously shown that iron phosphate glass compositions are highly tolerant towards LKE incorporation. Thus, we considered a modified base glass formulation, $10Na_2O–36Fe_2O_3–54P_2O_5$, for the development of an iron phosphate glass–monazite ceramic wasteform for lanthanide oxide fission product wastes produced from LKE salt clean-up. This could allow the Na_2O component to be substituted by $Li_{0.48}K_{0.52}Cl$, if desirable. In this preliminary study, we considered demonstration of a glass ceramic with the composition $(100–x)(10Na_2O–36Fe_2O_3–54P_2O_5)–xLa_2O_3$ ($x = 5$, 10, 15), with La_2O_3 as a surrogate for the lanthanide oxide waste stream (this is equivalent to 5, 10 and 15 mol% La_2O_3 incorporation in the base glass).

Materials and methods

Materials synthesis

An iron phosphate base glass (IPG), of composition $10Na_2O–36Fe_2O_3–54P_2O_5$ (mol%), was produced by melting stoichiometric quantities of Na_2CO_3, Fe_2O_3 and $NH_4H_2PO_4$. Batched material was melted for 4 h at 1100 °C and quenched into water to produce a frit of mm dimensions. The frit was mixed with La_2O_3 to produce a batches with 5, 10 and 15 mol% La_2O_3. Batched material was transferred to a recrystallized alumina crucible and melted for 4 h at 1100 °C. The melts were cast onto a steel plate, transferred to a furnace and annealed at 500 °C for 1 h before cooling at 1 °C min^{-1} to room temperature.

Materials characterisation

Synthesised glasses were characterised by powder X-ray diffraction (XRD). XRD was performed using a Bruker D2 Phaser diffractometer utilising Cu Kα radiation, utilising a Ni foil Kβ filter and a point step of 0.02 from 10° to 70° 2θ; the energy discriminator window of the position-sensitive Lynxeye detector was set to maximise the rejection of the fluorescent background.

Scanning electron microscopy coupled with energy-dispersive spectroscopy (SEM-EDX) was used to evaluate the microstructure and average composition of the synthesised glass-ceramics. Scanning electron microscopy (SEM) using a Hitachi TM3030 SEM equipped with a Bruker Quantax EDX. An accelerating voltage of 15 kV was used for imaging. Glass-ceramics were prepared for SEM analysis by mounting in cold setting resin and polishing with SiC paper and progressively finer diamond pastes to an optical finish (1 mm).

Results

Figure 1 shows the results of powder X-ray diffraction of the synthesised glass-ceramic. As can be seen, the target monazite phase was successfully synthesised for the 5 and 10 mol% La_2O_3-targeted compositions with no other crystalline phases evident in the diffraction pattern. The broad region of diffuse scattering from $20° < 2\theta < 40°$ indicates the presence of a glassy phase alongside the crystalline

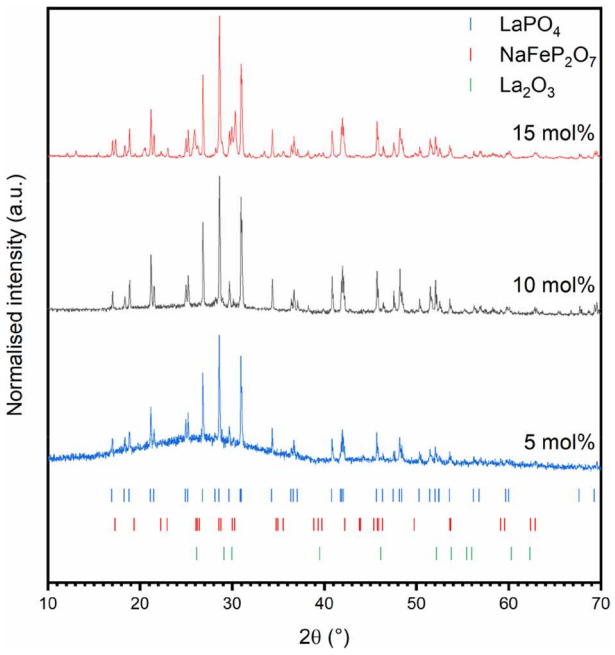

Fig. 1 X-ray diffraction patterns of synthesised glass-ceramics. Tick marks show allowed reflections for their respective phases (minimum 5% maximum intensity)

monazite. These results are similar to those reported by Wang et al. concerning the crystallisation of Nd and Gd monazites forms iron borophosphate glasses [9, 10]. The relative intensity of the monazite $LaPO_4$ reflections observed in this study is greater than those observed by Wang et al. for counterpart Ln_2O_3-loaded iron borophosphate glasses with Ln = Nd and Gd. Deng et al. found that the addition of CeO_2 to a $40Fe_2O_3$–$60P_2O_5$ iron phosphate base glass resulted in the formation of both $CePO_4$ and $FePO_4$ at incorporation rates as low as 4 mol% [12]. It would, therefore, appear that the addition of Na_2O in this study (and B_2O_3 in previous studies [9, 10]) stabilises the iron phosphate glass matrix against crystallisation of $FePO_4$. This is of significance, since the crystallisation of iron phosphate glass phases is known to adversely affect the durability of iron phosphate glasses, through loss of hydration-resistant Fe–O–P bonds [13]. The 15 mol% La_2O_3 sample was found to be highly crystalline, the target monazite phase was successfully formed alongside $FePO_4$, $NaFeP_2O_7$ and retained La_2O_3. It is hypothesised that the formation of a larger fraction of monazite fraction removes phosphorus from the glass network, destabilising it, resulting in gross crystallisation.

Asuvathraman et al. noted that the addition of 0.2 f.u. (formula units) Ca to $CePO_4$ resulted in a change in unit cell size and a measurable change in the lattice parameters of the target phase relative to stoichiometric $CePO_4$ [7]. The refined lattice parameters of the monazite phase (10 mol% sample) produced in this study are in excellent agreement with those previously published in the literature for stoichiometric $LaPO_4$ (Table 1) [14]. It is, therefore, unlikely that significant substitution of other ions into the monazite structure has occurred and the precipitated monazite is stoichiometric $LaPO_4$.

Table 1 Comparison of refined lattice parameters of synthesised monazite phase and published literature values

Lattice parameter	This study	Hirsch et al. [14]
a (Å)	6.8413(2)	6.841
b (Å)	7.0792(2)	7.076
c (Å)	6.5123 (3)	6.512
β (°)	103.267(2)	103.289

SEM-EDX observation of the synthesised samples was in agreement with XRD analysis, see Fig. 2. Micron-scale crystallites enriched in La and P were clearly visible in all three samples and were concluded to be monazite, $LaPO_4$. For the successful glass-ceramics (i.e. 5 and 10 mol% La_2O_3), observed monazite crystallites were in the size range of 1–10 µm, and it was also possible to observe a core of La_2O_3 oxide in some crystallites. EDX analysis of the crystallites and the matrix confirmed the presence of La in the crystalline phase and Na and Fe in the glass with P observed in both, as determined by X-ray emission lines. Point EDX measurements taken from the glass matrix and crystallites found distinct segregation of La from the matrix and little incorporation of Fe or Na in the monazite crystals, and the absence of substituent ions in the monazite phase was in agreement with the results of Rietveld refinement of XRD data.

The EDX data demonstrate partitioning of La from the glass to crystalline monazite $LaPO_4$ phase (Fig. 3), similar to that of monazite $GdPO_4$ and mixed (Ce, La, Nd)PO_4 in iron borophosphate glasses by Wang et al. [8, 10]. The substitution of Gd_2O_3 for Fe_2O_3 in the borophosphate base glass has been observed to result in an increase in the volume fraction of the monazite phase, as a result of greater lanthanide concentration, and also, it leads to a greater tendency for the glass matrix to crystallise [10]. Considering that the observed crystallisation behaviour and segregation of La from the glass phase, as determined by EDX (Fig. 3), it would appear likely that direct substitution of La_2O_3 for Fe_2O_3 would improve the relative yield of monazite but may increase the tendency of the glass matrix to crystallise due to the poorer glass-forming ability of La relative to Fe.

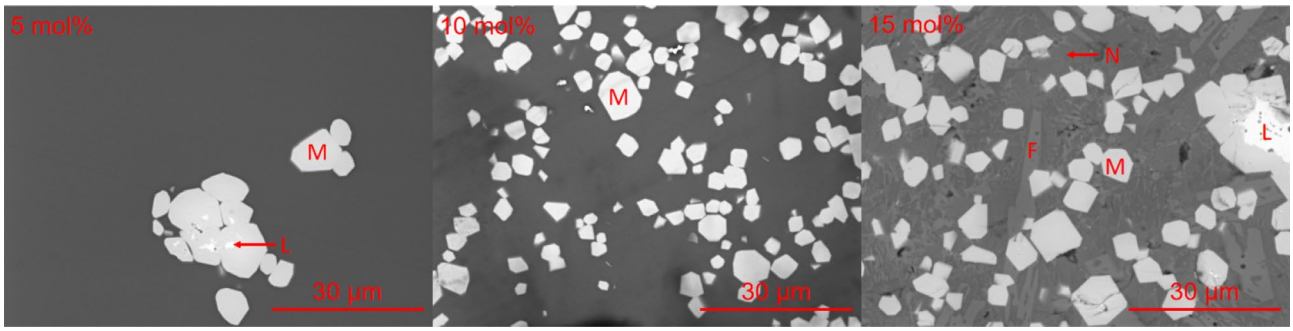

Fig. 2 Representative BSE images of 5, 10 and 15 mol% La_2O_3 glass-ceramics. M = monazite ($LaPO_4$), L = La_2O_3, F = $FePO_4$ and N = $NaFeP_2O_7$

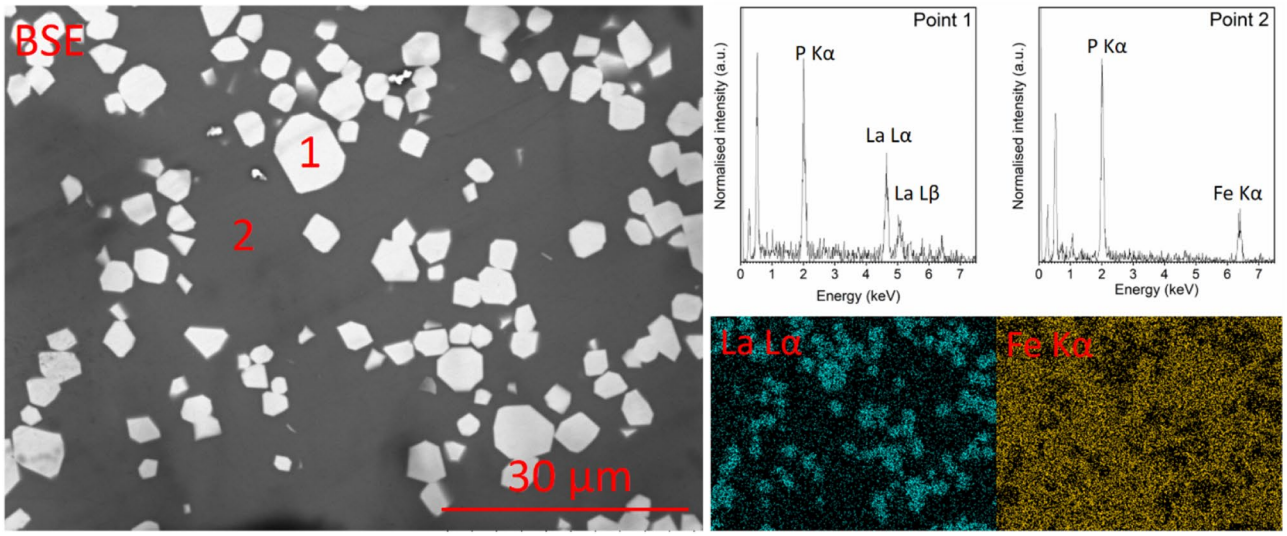

Fig. 3 BSE images and EDX analysis of crystallites and matrix materials for the 10 mol% La_2O_3 sample

Conclusions

This study has found that it is possible to produce monazite-alkali iron phosphate glass-ceramics via incorporation of La_2O_3 into a sodium iron phosphate base glass melting and annealing at 500 °C for 1 h. The synthesised glass-ceramic was found to contain distinct crystallites of 1–10 µm in size with clear segregation of La to the monazite phase. The formulation developed here demonstrated an Ln_2O_3 incorporation rate which marginally exceeds that previously achieved in iron borophosphate glasses. Partial crystallisation of the glass matrix, as observed at high Ln_2O_3 incorporation rates in iron borophosphate glasses, which is known to be detrimental to durability, was found to occur at higher substitution levels than observed previously. These data are very encouraging for further optimisation, through a more extensive systematic study of La_2O_3 incorporation rate and the extended phase diagram. The behaviour of more complex simulant Ln_2O_3 waste streams should also be investigated to understand the potential for fractionation of different Ln species between glass and ceramic phases.

Acknowledgments This research was funded under the £46m Advanced Fuel Cycle Programme as part of the Department for Business, Energy and Industrial Strategy's (BEIS) £505m Energy Innovation Programme and EPSRC under grants EP/S01019X/1 and EP/S011935/1. This research utilised the HADES/MIDAS facility at the University of Sheffield established with financial support from EPSRC and BEIS, under grant EP/T011424/1 [15].

Data availability The datasets generated during and/or analysed during the current study are available from the corresponding author on reasonable request.

Declarations

Conflict of interest The authors declare no conflict of interest relating to the publication of this work.

References

1. H.E. Garcia, M.J. Lineberry, S.E. Aumeier, H.F. McFarlane, Nucl. Plant J. **20**, 1–8 (2002)
2. R. Taylor, *Reprocessing and Recycling of Spent Nuclear Fuel*, vol. 2 (Woodhead Publishing, Cambridge, 2015)
3. Y.Z. Cho, G.H. Park, H.C. Yang, D.S. Han, H.S. Lee, I.T. Kim, J. Nucl. Sci. Technol. **46**, 1004–1011 (2009)
4. H. Hayashi, K. Minato, J. Phys. Chem. Solids **66**, 422–426 (2005)
5. Y. Castrillejo, M.R. Bermejo, R. Pardo, A.M. Martínez, J. Electroanal. Chem. **522**, 124–140 (2002)
6. B.J. Riley, Ind. Eng. Chem. Res. **59**, 9760–9774 (2020)
7. R. Asuvathraman, K. Joseph, R. Raja Madhavan, R. Sudha, R. Krishna Prabhu, K.V. GovindanKutty, J. Eur. Ceram. Soc. **35**, 4233–4239 (2015)
8. F. Wang, Y. Wang, Q. Liao, J. Zhang, W. Zhao, Y. Yuan, H. Zhu, L. Li, Y. Zhu, J. Non Cryst. Solids (2020). https://doi.org/10.1016/j.jnoncrysol.2020.120246
9. Y. Wang, F. Wang, Q. Wang, H. Zhu, G. Xiang, Q. Liao, Y. Zhu, J. Non Cryst. Solids **526**, 119726 (2019)
10. F. Wang, Q. Liao, Y. Dai, H. Zhu, J. Nucl. Mater. **477**, 50–58 (2016)
11. F. Wang, Q. Liao, K. Chen, S. Pan, M. Lu, J. Non Cryst. Solids **409**, 76–82 (2015)
12. Y. Deng, Q. Liao, F. Wang, H. Zhu, J. Nucl. Mater. **499**, 410–418 (2018)
13. C.W. Kim, C.S. Ray, D. Zhu, D.E. Day, D. Gombert, A. Aloy, A. Mogu, **322**, 152–164 (2012)
14. A. Hirsch, P. Kegler, I. Alencar, J. Ruiz-Fuertes, A. Shelyug, L. Peters, C. Schreinemachers, A. Neumann, S. Neumeier, H.P. Liermann, A. Navrotsky, G. Roth, J. Solid State Chem. **245**, 82–88 (2017)
15. N.C. Hyatt, C.L. Corkhill, M.C. Stennett, R.J. Hand, L.J. Gardner, C.L. Thorpe, I.O.P. Conf, Ser. Mater. Sci. Eng. **818**, 012022 (2020)